Modeling Electroporation in a Single Cell. I. Effects of Field Strength and Rest Potential

Katherine A. DeBruin, Ph.D. and Wanda Krassowska, Ph.D.
Department of Biomedical Engineering and Center for Emerging Cardiovascular Technologies, Duke University, Durham, North Carolina, USA

ABSTRACT This study develops a model for a single cell electroporated by an external electric field and uses it to investigate the effects of shock strength and rest potential on the transmembrane potential V_m and pore density N around the cell. As compared to the induced potential predicted by resistive-capacitive theory, the model of electroporation predicts a smaller magnitude of V_m throughout the cell. Both V_m and N are symmetric about the equator with the same value at both poles of the cell. Larger shocks do not increase the maximum magnitude of V_m because more pores form to shunt the excess stimulus current across the membrane. In addition, the value of the rest potential does not affect V_m around the cell because the electroporation current is several orders of magnitude larger than the ionic current that supports the rest potential. Once the field is removed, the shock-induced V_m discharges within 2 μs, but the pores persist in the membrane for several seconds. Complete resealing to preshock conditions requires approximately 20 s. These results agree qualitatively and quantitatively with the experimental data reported by Kinosita and coworkers for unfertilized sea urchin eggs exposed to large electric fields.

INTRODUCTION

Electroporation is the formation of microscopic, current-carrying pores in a lipid bilayer exposed to a large transmembrane potential V_m. The pores are long lived, often surviving in the membrane for up to several minutes and providing pathways for the movement of ions, drugs, and even DNA fragments into the cell. These properties have made electroporation a common tool in biotechnology (Chang et al., 1992; Neumann et al., 1989), and the medical applications of electroporation are now being realized (River et al., 1991; Tsong, 1991; Tung et al., 1995; Zhang et al., 1996).

However, the process of electroporation is not well understood. Numerous experimental studies have been aimed at revealing the mechanism of electroporation in various types of membranes ranging from artificial lipid bilayers (Chernomordik and Chizmadzhev, 1989; Glaser et al., 1988) to red blood cells (Chang, 1992; Kinosita and Tsong, 1979) to chick myocyte monolayers (Jones et al., 1978, 1987). These studies investigated the properties of pore formation and resealing using pulse charge techniques (Benz et al., 1979; Zimmermann, 1982), measured the kinetics of electroporation in voltage-clamped membranes (Chernomordik and Chizmadzhev, 1989; Tovar and Tung, 1992), tracked the movement of ions and fluorescent dyes across electroporated membranes (Kinosita et al., 1991; Mehrle et al., 1989; Rossignol et al., 1983), imaged the transmembrane potential using voltage-sensitive dyes (Hibino et al., 1993; Knisley, 1994), and visualized large pores using freeze-fracture electron microscopy (Chang, 1992). With the wide variety in membrane composition and experimental techniques, the literature on electroporation is difficult to compare and often conflicting. A model is needed to help understand the experimental results and draw qualitative, universal conclusions about the electroporation process and the behavior of electroporated cells.

Until recently, the development of theoretical models of electroporation has lagged behind the experimental research, with the available models unable to fully replicate or explain the experimental observations. The first model described the basic biophysics of electroporation using the Smoluchowski equation, which governs the evolution of the pore distribution function in the space of the pore radii (Pastushenko et al., 1979). Weaver and coworkers derived the equations of Pastushenko et al. from statistical mechanics and expanded the biophysical description into a numerical model (Barnett and Weaver, 1991; Freeman et al., 1994). However, these formulations are mathematically and computationally complex and therefore only suitable for use in space-clamped membranes. Recognizing the need to model electroporation in spatially extended systems, Weaver suggested a cubic cell model for electroporation that consists of two space-clamped membrane patches connected by a resistor (Weaver and Barnett, 1992). This representation captures some features of cellular electroporation, but it does not allow for spatial variation in the transmembrane potential or pore density.

The need for a model that provides a closer relationship between theory and experiments can be fulfilled by the macroscopic model of electroporation recently developed by DeBruin and Krassowska (1998), Krassowska (1995), and Neu and Krassowska (1999), which provides a means for investigating the mechanisms and effects of electroporation in a variety of tissue geometries. To date, the model has been used successfully to reproduce experimental re-

Received for publication 23 December 1998 and in final form 3 June 1999.
Address reprint requests to Katherine A. DeBruin, Ph.D., Department of Biomedical Engineering, Box 90281, Duke University, Durham, North Carolina 27708-0281. Tel.: 919-660-5131; Fax: 919-684-4488; E-mail: kad3@eel-mail.mc.duke.edu.
© 1999 by the Biophysical Society
0006-3495/99/09/1213/12 $2.00

sults involving guinea pig papillary muscle fibers exposed to large electric fields (DeBruin and Krassowska, 1998) and to investigate the influence of electroporation on the shock-induced transmembrane potential in a two-dimensional sheet of cardiac tissue (Aguel et al., 1999).

Part I of the present study uses the macroscopic model of electroporation as a basis for the development of a model of a single cell electroporated by an external electric field. This model is used to investigate the process of electroporation in a spherical cell, including the time evolution and spatial distribution of the transmembrane potential and pore density as well as the effects of the rest potential and shock strength. The modeling results are compared to experimental data reported in the literature.

METHODS

Mathematical Model

The transmembrane potential on the surface of an isolated single cell exposed to an external electric field can be computed using Laplace's equation, because both the intracellular and extracellular domains are source-free:

$$\nabla^2\Phi_i = 0 \quad \text{in intracellular space,} \tag{1}$$

$$\nabla^2\Phi_e = 0 \quad \text{in extracellular space,} \tag{2}$$

where Φ_i and Φ_e are the intracellular and extracellular potentials. The uniform external field E is included as a condition on Φ_e,

$$\Phi_e = -Er\cos\theta, \tag{3}$$

where r is the distance to the outer boundary of the extracellular space, and θ is the azimuthal angle (Fig. 1). The current density across the membrane S is given by

$$\begin{aligned} -\hat{n}\cdot(\sigma_i\nabla\Phi_i) &= -\hat{n}\cdot(\sigma_e\nabla\Phi_e) \\ &= C_m\frac{\partial V_m}{\partial t} + I_{ion} + I_{ep} \quad \text{on } S, \end{aligned} \tag{4}$$

where $\hat{n}$ is the unit vector normal to the membrane's surface, σ_i and σ_e are the intracellular and extracellular conductivities, C_m is the specific membrane capacitance, $V_m \equiv \Phi_i - \Phi_e$ is the transmembrane potential on the membrane, t is time, I_{ion} is the ionic current, and I_{ep} is the current due to electroporation. To focus on the effects of electroporation, the cell is assumed to have passive membrane kinetics in which I_{ion} can be described as

$$I_{ion} = g_l(V_m - E_l), \tag{5}$$

where g_l is the specific membrane conductance and E_l is the reversal potential of the ionic current. I_{ep} is the current due to the movement of ions through the shock-induced pores,

$$I_{ep} = Ni_{ep}, \tag{6}$$

where i_{ep} is the current through a single pore and N is the pore density. The current i_{ep} assumes that the pores provide pathways for the movement of generalized charges that are not identified as any particular ion species. A previously derived expression based on the Nernst–Planck equation models i_{ep} as an instantaneous function of the transmembrane potential (Barnett, 1990; DeBruin and Krassowska, 1998; Glaser et al., 1988),

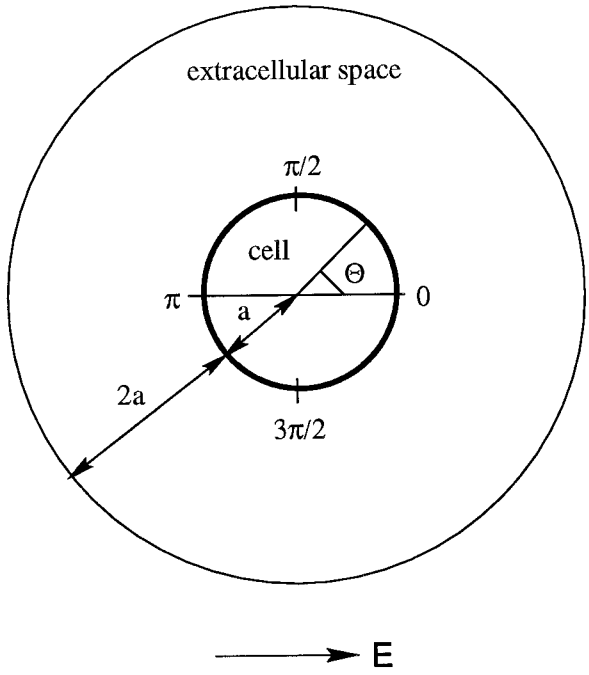

FIGURE 1 Schematic of a spherical single cell with radius a immersed in a spherical shell of extracellular space with thickness $2a$. The electric field E is oriented such that the depolarized pole is at $\theta = 0$ and the hyperpolarized pole is at $\theta = \pi$. All profiles of the transmembrane potential V_m or the pore density N around the cell are plotted from $-\pi/2$ to $3\pi/2$.

$$i_{ep} = \frac{\pi r_m^2\sigma v_m RT}{Fh} \cdot \frac{e^{v_m-1}}{\dfrac{w_o e^{w_o - nv_m} - nv_m}{w_o - nv_m}e^{v_m} - \dfrac{w_o e^{w_o+nv_m} + nv_m}{w_o + nv_m}}, \tag{7}$$

where r_m is the radius of the pore, σ is the conductivity of the aqueous solution that fills the pore, F is Faraday's constant, R is the universal gas constant, T is the absolute temperature, h is the thickness of the membrane, w_o is the energy barrier inside the pore, and n is the relative entrance length of the pore. The variable v_m is the nondimensional transmembrane potential, $v_m \equiv V_m(F/RT)$. In previous applications of Eq. 7 (DeBruin and Krassowska, 1998; Glaser et al., 1988), the energy barrier w_o accounted for the narrowing of the pore as it crosses the lipid bilayer as well as the electrical interactions between the ions and the pore wall. Therefore, the value of r_m in Eq. 7 was taken to be the size of the pore entrance, $h/2$. For this study, r_m denotes the radius of the narrowest part of the pore, so w_o reflects only the ion–wall interactions.

The pore density N is governed by a first-order differential equation (DeBruin and Krassowska, 1998; Neu and Krassowska, 1999),

$$\frac{dN}{dt} = \alpha e^{(V_m/V_{ep})^2}\left(1 - \frac{N}{N_o}e^{-q(V_m/V_{ep})^2}\right), \tag{8}$$

where N_o is the pore density when $V_m = 0$ mV, and α, V_{ep}, and q are constants. An explanation of the origin of Eq. 8 is given in Appendix A.

Method of Solution

For any cell shape, Eqs. 1–8 must be solved numerically. The intracellular and extracellular space is discretized using a finite difference method, and the resulting linear system of equations is transformed using LU decomposition. In each time step, the intracellular and extracellular potentials are computed using forward and backward substitution. The results are used to find V_m, I_{ion}, I_{ep}, and N at the present time step to be used in the calculation of Φ_i and Φ_e at the next time step. This approach solves the original problem described by Eqs. 1–4. An alternative approach is to use singular perturbation to derive an asymptotic approximation to those equations. By expanding the potentials in powers of a small parameter ε and using only the leading order terms, the time dependence of the boundary conditions disappears and Eqs. 1–4 become a quasi-stationary system that may be solved at widely spaced time intervals. In this case, changes in the transmembrane potential are driven by the time dependence in Eq. 8 for the pore density N. To achieve both accuracy and computational efficiency, this study developed a combined solution method in which Eqs. 1–4 are solved during the shock and the singular perturbation approximation is used during resealing. Additional details are given in Appendix B.

As an example, this study uses a spherical single cell with radius $a = 50\ \mu m$ immersed in a spherical shell of extracellular space with thickness $2a = 100\ \mu m$ (Fig. 1). Whenever possible, the cell parameters (diameter, passive kinetics), stimulus protocol (electric field strength, duration), material constants (intracellular, extracellular conductivities), and electroporation characteristics (significant effects at $V_m \approx 1$ V) are matched to the values reported by Kinosita and coworkers for unfertilized sea urchin eggs (Hibino et al., 1991, 1993; Kinosita et al., 1988, 1991, 1992). When a rest potential of −80 mV is required (Chambers and de Armendi, 1979), the reversal potential of the ionic current E_l is set to −83.75 mV. For a rest potential of 0 mV, E_l is set to 0 mV. The shock protocol consists of a 400-V/cm field applied for a duration of 1 ms. The electroporation parameters α, V_{ep}, N_o, and w_o appearing in Eqs. 7–8 depend on the type of membrane. For this study, the values of α, N_o, and w_o are based on experimental results from artificial lipid bilayers (Glaser et al., 1988), whereas the parameter V_{ep} was altered such that the critical transmembrane potential V_{cr} at which electroporation becomes significant is approximately 1 V. Values for all parameters are given in Table 1.

The constants V_{ep} and V_{cr} are related, but they are not equivalent. V_{ep} is a parameter in Eq. 8 indicating that the change in V_m causes an e-fold increase in the pore creation rate. Hence, V_{ep} is analogous to a time or length constant. If $V_m = V_{ep}$, then the pore creation rate changes by only a factor of $e^1 = 2.7$, too small to be detected experimentally. However, if $V_m = V_{cr} \approx 4V_{ep}$, then the pore creation rate changes by $e^4 = 55$, a factor large enough to cause an experimentally detectable change in the membrane conductance.

TABLE 1 Geometric, electrical, and electroporation parameters

Symbol	Value	Definition
a	50.0 μm	Cell radius
r_m	0.76 nm	Pore radius
h	5.0 nm	Membrane thickness
g_l	0.19 mS/cm^2	Specific membrane resistance
E_l	−83.75 mV	Reversal potential of ionic current
C_m	0.95 μF/cm^2	Specific membrane capacitance
σ_i	4.55 mS/cm	Intracellular specific conductivity
σ_e	50.0 mS/cm	Extracellular specific conductivity
T	295 K (22°C)	Temperature
σ	13.0 mS/cm	Conductivity of aqueous solution in pores
n	0.15	Relative entrance length of pores
q	2.46	Electroporation constant
α	100.0 cm^{-2} ms^{-1}	Electroporation parameter
V_{ep}	258 mV	Characteristic voltage of electroporation
N_o	1.5×10^5 cm^{-2}	Equilibrium pore density when $V_m = 0$ mV
w_o	2.65	Energy barrier within pore

Throughout the shock, Eqs. 1–4 are solved with a combined solution method using varying time steps. When the transmembrane potential of the cell is changing quickly (i.e., charging, discharging), the original equations are solved with a time step of $\tau_c/32 = 0.034\ \mu s$, where τ_c is the time constant of cellular polarization (Hibino et al., 1993),

$$\tau_c = aC_m\left(\frac{1}{\sigma_i} + \frac{1}{\sigma_e}\right) = 1.1\ \mu s. \tag{9}$$

After the initial transient ($8\tau_c = 9\ \mu s$ for a 400-V/cm field), V_m and N change slowly and the time step is increased to $\tau_c/4 = 0.28\ \mu s$. Once the shock is terminated and the cell discharges, the resealing process is captured with the singular perturbation approximation and a time step of 100 ms. Eq. 8, for the pore density, is solved using Euler's method throughout the simulation. The spatial discretization of the cell uses 64 nodes over one-half of the sphere's circumference and, in the radial direction, uses 10 nodes within the cell and 20 nodes within the extracellular space. Simulations were run on a Sun Ultra 1 workstation.

RESULTS

RC Cell versus Electroporating Cell

According to the literature, a spherical cell with a passive resistive-capacitance (RC) membrane exposed to an external electric field will polarize such that the maximum and minimum transmembrane potentials V_m occur at the poles of the cell, and V_m at the equator is equal to the rest potential V_{rest} (Schwann, 1989). The polarization arises with a time constant of $\tau_c = 1.1\ \mu s$ (Eq. 9), and the time course of V_m is consistent with the exponential charging expected of an RC membrane (Fig. 2 *A*, *dashed line*). Once charging is complete, the transmembrane potential varies cosinusoidally around the circumference of the cell according to the relationship

$$V_m = \tfrac{3}{2}Ea\cos\theta, \tag{10}$$

where E is the electric field strength, a is the radius of the sphere, and $V_{rest} = 0$ mV is assumed (Fig. 2 *B*, *dashed line*). This result has been verified experimentally for small shocks, i.e., $|V_m| < 300$ mV (Gross et al., 1986; Lojewska et al., 1989).

However, when a cell is exposed to a shock that induces larger transmembrane potentials, electroporation occurs and the RC theory fails. The V_m charging transient is interrupted, and the transmembrane potential settles into a nearly constant value of approximately 1 V, the critical value of transmembrane potential V_{cr} required to produce significant electroporation in this preparation (Fig. 2 *A*). At the end of a 1-ms shock, the transmembrane potential profile around an electroporated cell is smaller than the profile predicted for an RC cell (Fig. 2 *B*). The largest decrease in V_m occurs at the poles where the induced potential is largest, and the smallest decrease is near the equator. The profile has also lost its cosinusoidal shape, appearing flattened as approximately two-thirds of the cell's circumference has a nearly uniform V_m magnitude of $V_{cr} \approx 1$ V.

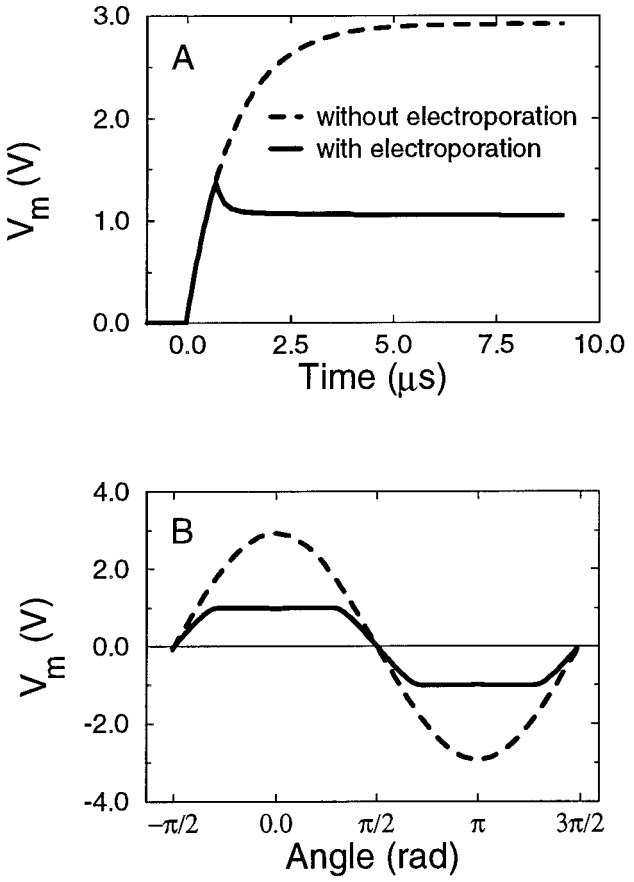

FIGURE 2 (*A*) Time course of the transmembrane potential V_m at the depolarizing pole of a spherical cell exposed to a 400-V/cm field. The nonelectroporating single cell (*dashed line*) charges to its steady-state value with a time constant $\tau_c = 1.1$ μs, but the charging of the electroporating cell (*solid line*) is interrupted within 1 μs of shock application and V_m settles into a constant value of approximately 1 V. (*B*) V_m around the cell at the end of a 400-V/cm, 1-ms shock. The transmembrane potential for the nonelectroporating cell (*dashed line*) shows the cosinusoidal shape predicted by RC theory. V_m around the electroporated cell (*solid line*) is lower and the profile is flattened in the polar regions.

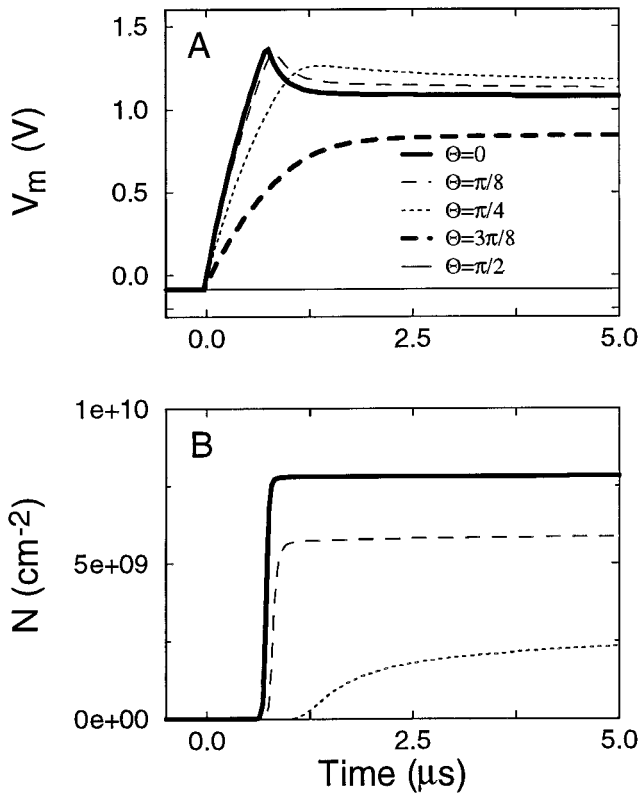

FIGURE 3 Time course of (*A*) V_m and (*B*) N at five locations around a spherical cell. Near the poles ($\theta = 0, \pi/8$), the V_m transient is initially steep but quickly truncated, and N experiences almost a step increase once V_m exceeds the critical value for electroporation $V_{cr} \approx 1$ V. Near the equator, where the induced potentials are smaller ($\theta = 3\pi/8, \pi/2$), V_m follows the time course for an RC cell. Since $V_m \ll V_{cr}$, there is no significant increase in N in that region.

Time Evolution of V_m and N

This dramatic change in the electrical behavior of the cell can be explained with a detailed examination of the time courses of V_m and the pore density N. When exposed to an electric field, the cell initially polarizes with a cellular time constant $\tau_c = 1.1$ μs. Near the equator, where the induced potential is less than the critical value for electroporation V_{cr}, the membrane will polarize to the steady-state potential predicted for an RC cell (Fig. 3 *A*, $\theta = 3\pi/8, \pi/2$). The membrane in this region will contain a small, baseline number of pores (e.g., N_o at $V_m = 0$ mV), but N does not change significantly during charging (Fig. 3 *B*) and the current through these pores does not influence V_m. Near the poles, the transmembrane potential quickly exceeds the critical value for electroporation ($V_{cr} \approx 1$ V) and creates a very fast increase in the pore density N (Fig. 3, $\theta = 0, \pi/8$). A portion of the stimulus current is shunted across the membrane through these pores, interrupting the V_m charging transient within about 1 μs of exposure to the electric field. In the region between the pole and the equator ($\theta = \pi/4$), the increase in N is more gradual because the induced potential is smaller.

After the charging transient, N in the electroporated regions of the cell settles into a slow upward drift because V_m is still greater than V_{cr}. This continued creation of pores provides additional pathways to shunt current across the membrane, and V_m throughout the electroporated region slowly decreases toward V_{cr}. This feedback between V_m and N occurs at different rates in different locations. Near the poles, the V_m transients are steeper and create larger pore densities than in the surrounding regions (Fig. 3). With more current pathways across the membrane, the post-transient transmembrane potential is smaller. This situation can be observed at the end of the 5-μs shock shown in Fig. 3 *A*, where the transmembrane potential at the pole ($\theta = 0$) is smaller than V_m at $\theta = \pi/8$, which is, in turn, smaller than V_m at $\theta = \pi/4$. At the $\theta = 3\pi/8$ location, the transmembrane potential is subcritical and no electroporation occurs.

The post-transient differences in V_m create concavities, or dips, in the transmembrane potential distribution around the

cell (Fig. 4 *A*). The magnitude of these concavities decreases over time as N compensates by increasing nonuniformly (Fig. 4 *B*). At the end of a 1-ms shock, V_m is nearly constant at 1 V throughout the electroporated regions (Fig. 4 *A*, *heavy solid line*). The transmembrane potential may be considered symmetric about the equator, because the magnitude of V_m is the same at the depolarized and hyperpolarized ends of the cell. The pore density N is also symmetric.

Rest Potential

Theory applicable to RC cells predicts that the intrinsic rest potential V_{rest} of the cell will alter the transmembrane potential profile by shifting it in the direction of V_{rest}. V_m at the poles would still be symmetric about the equator, but the transmembrane potential at that location would be equal to the rest potential. For example, if $V_{rest} = -80$ mV, then the cell in this study would have V_m equal to +2.92 V at the depolarized pole and −3.08 V at the hyperpolarized pole, both 3 V from the rest potential. However, in this scenario, the transmembrane potentials still far exceed the critical potential for electroporation, $V_{cr} \approx 1$ V, so significant electroporation will occur at both ends of the cell. Intuitively, one would expect that the negative bias of the rest potential would cause the hyperpolarized end to electroporate earlier than the depolarized end, and the correspondingly steeper slope of the V_m transient would produce a larger pore density. Since the cell is a source-free system (Eq. 1), the net transmembrane current must be zero under all conditions (Krassowska and Neu, 1994). After the first 1–2 μs, the capacitive transient is complete, and the electroporation current is much larger than the ionic current. Therefore, one would also expect that V_m at the hyperpolarized end would be smaller than at the depolarized end.

Comparing V_m and N at points around the cell at the end of a 400-V/cm, 1 ms shock confirms that intuitive scenario qualitatively (Table 2). With $V_{rest} = -80$ mV, the pore density at the hyperpolarized pole is larger than N at the depolarized pole, while the opposite is true for the magnitude of V_m. Quantitatively, the asymmetry in V_m and N is very small, and it is unlikely that this minor variation would be detectable experimentally. However, Table 2 also shows a surprising result that can be measured experimentally: V_m at the equator ($\theta = \pi/2$) is approximately equal to 0 mV even if the intrinsic rest potential of the cell is −80 mV. This negative offset disappears during the initial charging transient because the nearly step increase in N increases the electroporation current I_{ep} by four orders of magnitude, making $I_{ep} \gg I_{ion}$, the ionic current that supports the rest potential. The electrical behavior of the cell is governed by I_{ep}, even in regions which are not electroporated. The intrinsic rest potential of the cell plays only a minor role, producing the slight asymmetry in V_m and N observed in Table 2.

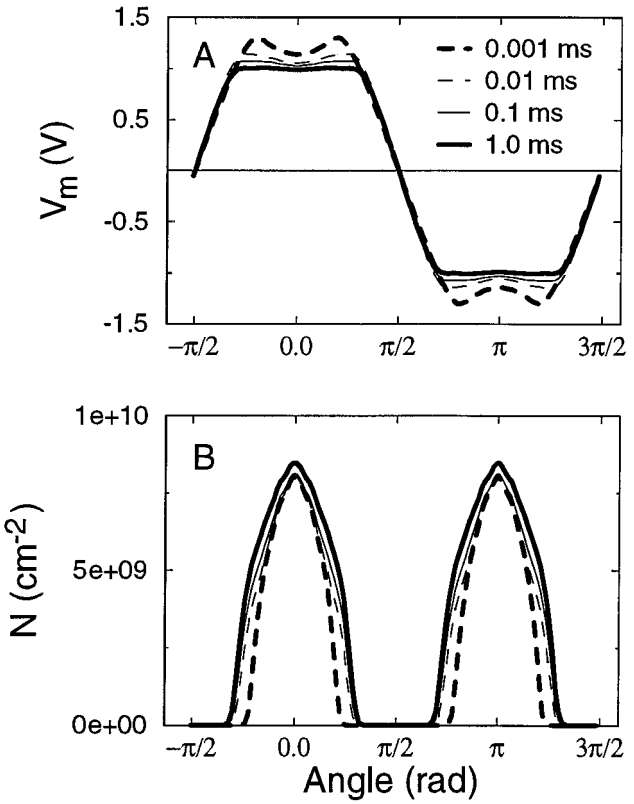

FIGURE 4 (*A*) V_m and (*B*) N around a spherical cell for four time instants during a 1-ms shock. The concavity in V_m near the poles disappears over time, while the pore density distribution gradually widens and increases.

Field Strength

The bimodal shape of the pore density distribution around the cell (Fig. 4 *B*) is directly related to the cosinusoidally varying magnitude of the transmembrane potential initially induced by the electric field. Larger potentials, such as those near the poles, produce more pores to shunt the extra stimulus current across the membrane. Near the equator, the subcritical V_m does not significantly influence N. Increasing the electric field strength will increase the number of pores throughout the cell in an effort to dissipate the extra stimulus current, and a larger fraction of the cell membrane will attain the critical transmembrane potential V_{cr} and electroporate. However, the shape of the pore density distribution

TABLE 2 Effect of rest potential on electroporation

Parameter	Location	$V_{rest} = 0$ mV	$V_{rest} = -80$ mV
V_m (mV)	0	989.37	992.73
	$\pi/2$	0.00	0.10
	π	−989.37	−981.75
N (cm^{-2})	0	8.49×10^9	8.36×10^9
	$\pi/2$	1.50×10^5	1.94×10^5
	π	8.49×10^9	8.57×10^9

and the transmembrane potential are qualitatively unchanged (Fig. 5).

The exception to this behavior occurs when the cell is exposed to a shock that induces transmembrane potentials just over V_{cr}. For example, if the cell in this study is exposed to a 150-V/cm field, the maximum RC transmembrane potential equals 1.125 V instead of the usual 3 V. With the smaller field strength, the initial transient in V_m is less steep, fewer pores are formed, and the initial bias in pore density produced by the rest potential becomes important. Figure 6 shows the time course of V_m and N at both poles during a 150-V/cm shock. The hyperpolarized pole electroporates first because of the negative value of V_{rest}, and N in that region increases by approximately three orders of magnitude (Fig. 6 *B*, *dashed line*). The pore density at the depolarized pole is still small because $V_m < V_{cr}$. If the shock ended during this time frame (duration less than 80 μs), there would be a significant asymmetry in the pore density profile. As V_m at the hyperpolarized pole becomes less negative, the balance of current increases V_m at the depolarized pole. For shock durations between 100 μs and 240 μs, N at the depolarized pole is larger as the increasing V_m causes that end of the cell to electroporate. For shocks longer than about 240 μs, the difference in N at the two poles become less significant, and, after 500 μs, both the transmembrane potential and the pore density are almost symmetric. These results imply that shock strength and rest potential may be important, but only when the cell is polarized to just over the critical V_m with shocks of very short duration. Larger or longer shocks eliminate the effects of V_{rest}.

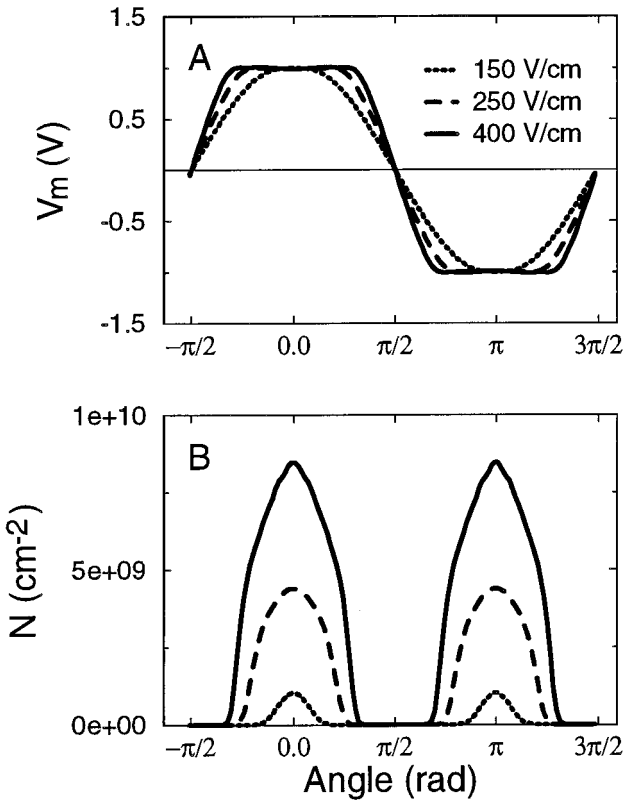

FIGURE 5 (*A*) V_m and (*B*) N around a spherical cell at the end of a 1-ms exposure to three electric field strengths. Larger fields did not alter the maximum magnitude of V_m, but did increase the height and width of the pore density profile. As a result, the fraction of the cell membrane with $V_m \approx 1$ V also increased.

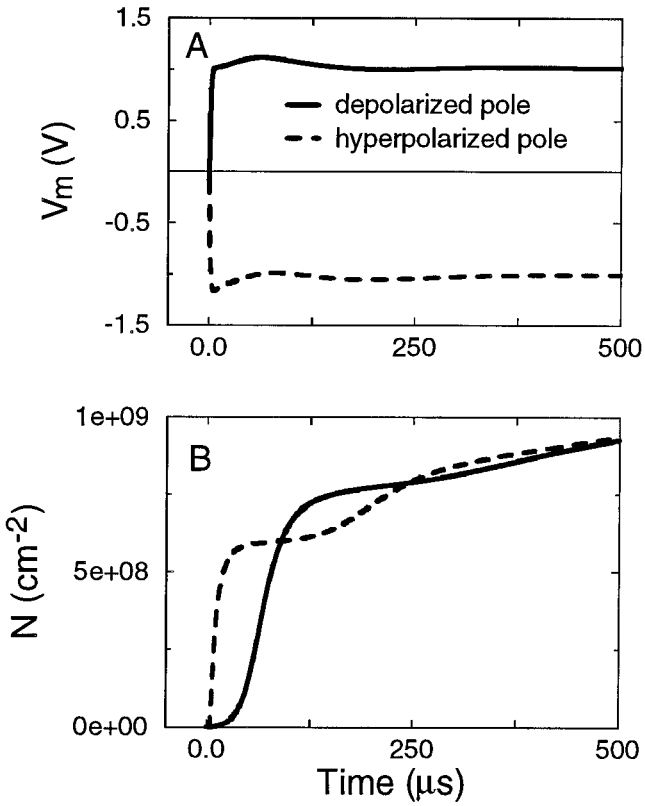

FIGURE 6 Time course of (*A*) V_m and (*B*) N at the poles of a spherical cell exposed to an electric field of 150 V/cm. This field induces potentials that barely exceed the critical value of electroporation, $V_{cr} \approx 1$ V, at the poles of the cell. V_m experiences some minor fluctuations around V_{cr}, but the time course of N shows that electroporation at the depolarized pole is delayed by 80 μs with respect to the hyperpolarized pole. If the shock were terminated during this time period, a very asymmetric pore density profile could be obtained. After 500 μs, N is almost identical at each pole.

Resealing

When the shock ceases, the cell discharges the potential induced by the electrical field. This process is faster than cellular polarization because electroporation increases the total conductance of the membrane. If $V_{rest} = 0$ mV, the transmembrane potential around the cell discharges to zero within a few microseconds. If $V_{rest} = -80$ mV, V_m follows a similar time course, discharging to a value very close to 0 mV within 1–2 μs. The cell requires about 20 s to return to its preshock conditions (Fig. 7).

The cell's prolonged recovery period is due to the slow rate of pore resealing, whose time constant can be evaluated

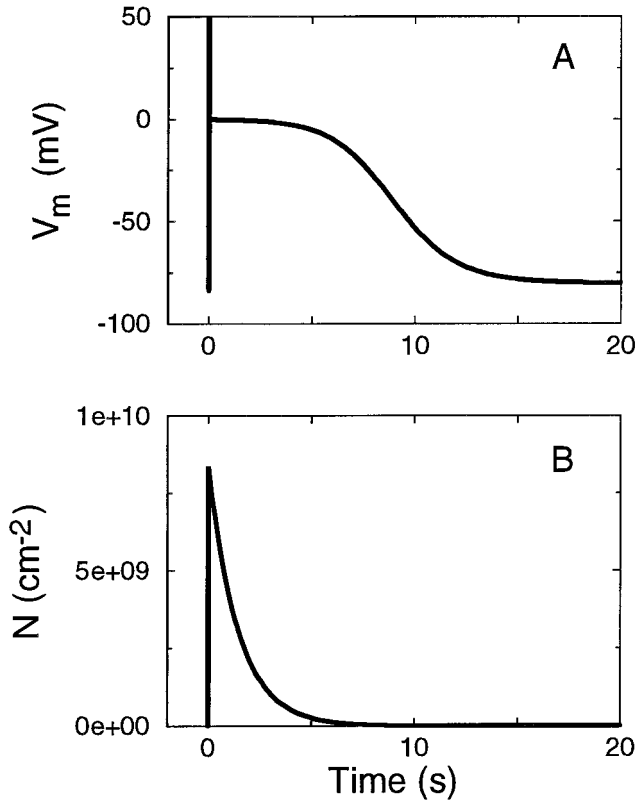

FIGURE 7 Time course of (*A*) V_m and (*B*) N at the depolarized pole of the cell after a 400-V/cm, 1-ms shock. The vertical line in panel *A* is the V_m trace during the shock, which appears very short on a time scale of many seconds. V_m slowly repolarizes to its rest potential of −80 mV over a period of 20 s, the time required for the pores to completely reseal and N to return to its preshock value throughout the cell.

from Eq. 8,

$$\tau_N = \frac{N_o}{\alpha} e^{(q-1)(V_m/V_{ep})^2}. \quad (11)$$

For $V_m = 0$ mV, $\tau_N = N_o/\alpha = 1.5$ s. The pore density decreases exponentially and requires approximately 20 s to return to its preshock distribution (Fig. 7 *B*). The slow decrease in N keeps V_m elevated because the electroporation current $I_{ep} \propto N$ is still large even after the shock has ended. The electrical behavior of the cell is dominated by I_{ep}, which has a reversal potential of 0 mV. As the pores reseal, I_{ep} decreases and becomes comparable to the magnitude of the ionic current I_{ion} that supports the rest potential. As N returns to its preshock value, I_{ion} dominates the transmembrane current and reestablishes the cell's intrinsic rest potential of −80 mV.

DISCUSSION

This study developed a computationally efficient model of a spherical single cell with an electroporating membrane. The modeling results demonstrate that electroporation substantially alters the transmembrane potential around the cell. As compared to V_m predicted for an RC cell, electroporation decreases the transmembrane potential throughout the cell and flattens the predicted cosinusoidal profile near the poles. The pore density increases with shock strength such that V_m in the electroporated regions remains nearly constant at 1 V regardless of the strength of the applied electric field. After the shock, the pores reseal with a time constant of 1.5 s, and complete recovery of the cell to preshock conditions requires approximately 20 s. The intrinsic rest potential of the cell was found to have essentially no effect on either V_m or N.

Comparison to Experimental Results

The majority of results reported in this study are similar to experimental observations made by Kinosita and coworkers, who used a voltage-sensitive fluorescent dye to investigate the transmembrane potential induced in unfertilized sea urchin eggs exposed to large electric fields (Hibino et al., 1991, 1993; Kinosita et al., 1988, 1991, 1992). First, the researchers observed that the transmembrane potential throughout the cell was much lower than predicted for an RC cell, similar to the modeling results shown in Fig. 2 *B* of this study. The experimental profile of V_m showed a flattening in the polar regions, and a concavity existed at both poles. However, in contrast to Fig. 4 *A* of this modeling study, the degree of concavity did not appear to decrease over time. Kinosita and coworkers also found that significant electroporation occurred during the first microsecond of the shock, followed by a slower increase in the electroporation conductance throughout the duration of the shock. This qualitative description of the time course of N agrees with the model's predictions (Fig. 4 *B*), but V_m has more complicated behavior experimentally. This discrepancy may be due to changes in the radii of pores during the shock, a feature not presently included in the model of electroporation. In experiments, the maximum electroporation conductance G decreased by an order of magnitude within the first millisecond postshock, and resealing was not complete after 2 s (the longest time interval measured). These results are also consistent with the predictions of this modeling study, in which G at the poles decreased by 85% in the first postshock millisecond because of the non-ohmic nature of the pores, and complete resealing to preshock conditions requires 20 s. A similar time course for electroporation was reported for green algae cells (Neumann et al., 1992).

Second, Kinosita's group tested the saturation of the transmembrane potential with shock strength and found that, for sufficiently large shocks, increasing the field strength did not increase V_m. This observation is consistent with the modeling results indicating that larger shocks create more pores, shunting the excess stimulus current across the membrane and limiting V_m to approximately 1 V throughout the electroporated region (Fig. 5). Knisley found a similar relationship in his study of rabbit myocytes (Knisley, 1994), in which larger shocks produced a more pro-

nounced decay in V_m such that the transmembrane potential at the end of a 20-ms shock was approximately equal for all field strengths. This saturation of V_m appears to be a phenomenon that is independent of tissue geometry, because it was also observed in both experimental and modeling studies of voltage-clamped lipid bilayers (Freeman et al., 1994), one-dimensional fibers (DeBruin and Krassowska, 1998; Krassowska, 1995; Zhou et al., 1996), and two-dimensional sheets (Aguel et al., 1999).

Third, Kinosita and coworkers observed a disappearance of the rest potential consistent with the modeling results (Table 2). Other researchers (Knisley and Grant, 1995; Teruel and Meyer, 1997) also found that the intrinsic rest potential did not play an important role in the electroporation process. These two experimental studies eliminated the intrinsic V_{rest} by altering the extracellular ionic concentrations, but the results were the same as those observed with a negative rest potential.

Finally, Kinosita's group estimated the electroporation conductance G based on their experimental data and reported a maximum G of 4.3×10^3 mS/cm^2. The distribution of the electroporation conductance around the cell was bimodal, with the largest value of G at either pole and a small value near the equator. The modeling study produced similar results, with a maximum G of 2.2×10^3 mS/cm^2 and a pore density distribution with a qualitatively similar shape (Fig. 4 *B*). Both model and experiment found that approximately two-thirds of the cell are significantly electroporated with an electric field strength of 400 V/cm. Kinosita and coworkers also calculated the maximum fractional area of the membrane occupied by the pores to be 10^{-4} to 10^{-3}, consistent with the experimentally and theoretically determined values for artificial lipid bilayers reported in the literature (Chernomordik et al., 1983; Freeman et al., 1994). This modeling study predicts that the fractional area of the example cell occupied by pores is 2×10^{-5}, again in agreement with the experimental results.

Comments

The steep dependence of the pore creation rate (Eq. 8) on the transmembrane potential is inherent to the electroporation process and cannot be avoided by choosing different electroporation parameters. For example, manipulating α and N_o within a physiologically valid range (α, 92 cm^{-2} ms^{-1} [Glaser et al., 1988] to 200 cm^{-2} ms^{-1} [DeBruin and Krassowska, 1998]; N_o, 1.5×10^4 to 1.5×10^6 cm^{-2} [Benz and Hancock, 1981; Chernomordik and Chizmadzhev, 1989; Rosenberg and Jendrasiak, 1968]) will not significantly alter the dependence, because the rate of change of the pore density is not strongly affected by either of these parameters. In comparison, dN/dt is exponentially dependent on V_{ep}, but altering that parameter will change the value of the critical transmembrane potential V_{cr}, which is determined by experimental data for a particular cell type.

This steep dependence of dN/dt on V_m has two consequences. First, at equilibrium, V_m is the square root of a logarithmic function of N, implying that V_m is almost insensitive to changes in N. This relationship explains the saturation phenomena observable in Fig. 5, where increasing the shock strength from 150 V/cm to 400 V/cm increased N by a factor of 8.2, but left V_m in the electroporated regions unchanged. Second, the increase in N is a very fast process, and the creation of pores is complete within about 1 μs (Fig. 3). This feature of the model does not necessarily contradict the experimental results that show electroporation occurs on a millisecond time frame (Hibino et al., 1993) and the critical transmembrane potential V_{cr} decreases with shock duration (Hibino et al., 1993). Instead, it is possible that the slow (millisecond) change in membrane conductance observed experimentally is due to an increase in the radii of the pores, a feature not represented in this model of electroporation. Likewise, the decrease in V_{cr} for longer pulses may be due to an increase in the pore radius, which increases the current through each pore and decreases V_m below V_{cr}. Including the effects of pore radius requires a substantial addition to the model that will be the subject of a future study.

Although the model of an electroporating cell successfully reproduced the experimental data published by Kinosita and coworkers (Hibino et al., 1991, 1993; Kinosita et al., 1988, 1991, 1992), it does have additional limitations. First, the model is a simplified description of the extremely complex processes occurring in a cell membrane. Important biophysical elements such as the stretching of cells exposed to an electric field (Isambert, 1998) are not captured. Second, the value of the electroporation parameter V_{ep} was chosen to give a critical V_m for electroporation of ± 1 V (value reported by Kinosita's group), but the values of other parameters were estimated from experiments performed on artificial lipid bilayers and therefore may not be wholly applicable to sea urchin eggs. Third, the macroscopic model of electroporation describes only primary pores, those formed as a direct result of large transmembrane potentials. Secondary pores, which are thought to be a later stage of development that provides transport routes for macromolecules including DNA (Weaver and Chizmadzhev, 1996), are beyond the scope of this model. Finally, the pores have been shown experimentally to be cation selective (Weaver and Chizmadzhev, 1996), but that feature is not included in this model of electroporation.

Despite these limitations, the only significant difference between the experimental results from Kinosita and coworkers and the modeling results reported here concerns the asymmetry of the electroporation process. The majority of Kinosita's studies show that the transmembrane potential is symmetric around an electroporated cell (Hibino et al., 1991; Kinosita et al., 1988, 1992), but the most recent experiments indicate that there may be a transient asymmetry in V_m when the shock is first applied (Hibino et al., 1993). More studies of the transmembrane potential are needed, but many researchers have reported an asymmetry in the uptake of marker molecules with entry predominately at the hyperpolarized end of the cell (Djuzenova et al., 1996;

Gabriel and Teissie, 1997; Knisley and Grant, 1995; Mehrle et al., 1985, 1989; Rossignol et al., 1983; Tekle et al., 1990; Teruel and Meyer, 1997). Several studies attribute this asymmetry in uptake to the rest potential, because the negative value is thought to bias electroporation toward the hyperpolarized pole (Djuzenova et al., 1996; Gabriel and Teissie, 1997; Mehrle et al., 1985, 1989; Tekle et al., 1990). The findings of this modeling study imply that this hypothesis is only valid when the induced potential is very near the critical value for electroporation (Figs. 5 and 6). All the experimental studies quoted here use electric fields that far exceed the critical value, and, in those cases, the model predicts that V_{rest} will cause only a very minor asymmetry in the transmembrane potential and the pore density. Thus, these modeling results rule out V_{rest} as a cause of the asymmetric uptake of marker molecules.

Other factors must be considered to explain this experimentally observed asymmetry. First, the lipid bilayer itself may be asymmetric, in which case the polarity of the shock would affect the local creation of pores (Genco et al., 1993). Second, there may be interactions between the pores and the ionic channels, proteins, and other structures in the membrane that are not replicated by the model. Finally, electroporation may be influenced by different ionic concentrations in intracellular and extracellular space (Djuzenova et al., 1996; Knisley and Grant, 1995; Tekle et al., 1994). This last hypothesis will be investigated theoretically in Part II of this study, which focuses on the interaction between electroporation and ionic concentrations (DeBruin and Krassowska, 1999).

APPENDIX A: ORIGIN OF EQ. 8 GOVERNING PORE DENSITY

This Appendix shows the connection between Eq. 8, used in this paper to compute the pore density, and the existing theory of electroporation. It is based on the results of a study by Neu and Krassowska (1999), who derived Eq. 8 as an asymptotic limit of the Smoluchowski equation, generally recognized in the literature as describing the biophysical mechanisms of electroporation.

Neu and Krassowska assumed a relationship between the pore radius and the pore energy that was proposed by Chizmadzhev and colleagues (Abidor et al., 1979; Glaser et al., 1988). As shown in Fig. A1, the energy $E(r)$ of a pore with radius r is the lesser of the two curves,

$$E(r) = E_*\left(\frac{r}{r_*}\right)^2, \tag{A1}$$

the energy of nonconducting (hydrophobic) pores, and

$$E(r) = 2\pi\gamma r - \pi\sigma r^2 + \left(\frac{C}{r}\right)^4, \tag{A2}$$

the energy of conducting (hydrophilic) pores. In Eqs. A1–A2, r_* and E_* are the minimum radius and energy barrier for the creation of conducting pores (Fig. A1), γ is the pore edge energy, σ is the membrane surface tension, and C is a constant. The third term in Eq. A2 represents the steric repulsion between the lipid heads lining the pore (Israelachvili, 1992) and is responsible for the increase in pore energy with shrinking radius (Weaver and Chizmadzhev, 1996).

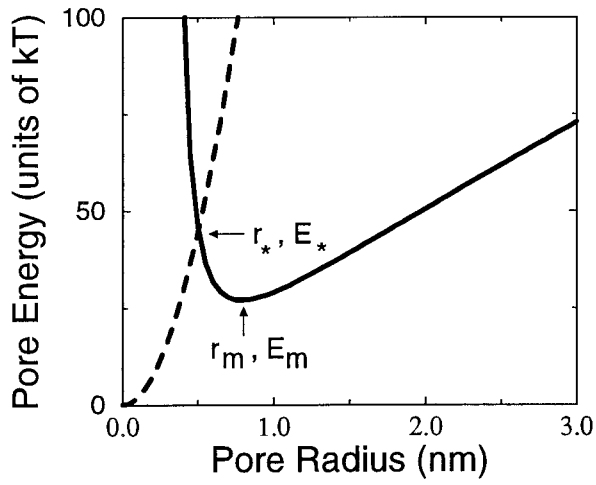

FIGURE A1 The energy of a pore as a function of radius at the transmembrane potential V_m = 0 mV. The dashed and solid lines show the energy of hydrophobic and hydrophilic pores, respectively. To better illustrate the relationship between the two pore types, the plot shows the pore energies only for small pore radii.

The pore energy $E(r)$ in Fig. A1 corresponds to the situation when there is no externally applied transmembrane potential. In the presence of a transmembrane potential V_m, the pore energy, denoted by $\varphi(r)$, is given by

$$\varphi(r) = E(r) - \pi a_p V_m^2 r^2, \tag{A3}$$

where the term $-\pi a_p V_m^2 r^2$ is the capacitive contribution (Abidor et al., 1979; Weaver and Mintzer, 1981). The coefficient a_p can be estimated based on a continuum model as (Glaser et al., 1988; Powell and Weaver, 1986)

$$a_p = \frac{1}{2h}(\kappa_w - \kappa_m)\epsilon_o, \tag{A4}$$

where h is the membrane thickness, κ_w and κ_m are dielectric constants of water and membrane, and ϵ_o is the permittivity of a vacuum.

Given the pore energy, electroporation is described mathematically by the Smoluchowski equation (Barnett and Weaver, 1991; Freeman et al., 1994; Pastushenko et al., 1979; Powell and Weaver, 1986; Weaver and Mintzer, 1981). If $n(r, t)$ denotes the pore density distribution function such that at a given time t, the number of pores per unit area with radii between r and $r + dr$ is $n(r, t)dr$, then $n(r, t)$ is governed by the equation,

$$\frac{\partial n}{\partial t} + D\frac{\partial}{\partial r}\left(-\frac{n}{kT}\frac{\partial \varphi}{\partial r} - \frac{\partial n}{\partial r}\right) = S(r), \tag{A5}$$

where D is the diffusion coefficient of pores, k is the Boltzmann constant, T is the absolute temperature, and $S(r)$ is the source term that represents the creation and destruction of pores. $S(r)$ can be written as

$$S(r) = \nu_c h \frac{U_r}{kT} e^{U/kT} - \nu_d n H(r_* - r), \tag{A6}$$

where ν_c is the attempt rate density (Weaver and Mintzer, 1981), ν_d is the frequency of lipid fluctuations (Glaser et al., 1988), and U denotes the pore energy φ of nonconducting pores ($r < r_*$). $H(r)$, the Heavyside step function, represents the fact that only nonconducting pores are destroyed.

The Smoluchowski equation (Eq. A5), used with constants typical for electroporation, contains several small parameters. Their presence facilitates the use of singular perturbation to perform a rigorous simplification of Eq. A5, and such an asymptotic reduction (Neu and Krassowska, 1999) transformed the Smoluchowski equation into an ordinary differential equa-

tion (ODE). This ODE describes the dynamics of the pore density $N(t)$, which is related to the pore distribution function $n(r, t)$ by

$$N(t) \equiv \int_{r_*}^{\infty} n(r, t)\, dr. \tag{A7}$$

The asymptotic ODE for $N(t)$ has the form

$$\frac{dN}{dt} = K\left(1 - \frac{N}{N_{eq}}\right). \tag{A8}$$

In the quasistatic case, K and N_{eq} are given by Eqs. 77–78 of the paper by Neu and Krassowska,

$$K = \alpha \exp[(V_m/V_{ep})^2], \tag{A9}$$

$$N_{eq} = N_o \exp[q(V_m/V_{ep})^2]. \tag{A10}$$

Substituting Eqs. A9 and A10 into Eq. A8 yields Eq. 8 used in the main body of this paper.

The paper of Neu and Krassowska relates the coefficients of Eqs. A8–A10 to constants appearing in the expressions for pore energy (Eqs. A1–A3) and in the Smoluchowski equation (Eq. A5–A6) (Neu and Krassowska, 1999):

$$\alpha = \frac{\nu_d}{r_*^2} \frac{|\varphi_*'|}{U_*' + |\varphi_*'|} e^{-E_*}, \tag{A11}$$

$$V_{ep} = \frac{1}{r_*} \sqrt{\frac{kT}{\pi a_p}}, \tag{A12}$$

$$N_o = \frac{1}{U_*' + |\varphi_*'|} \frac{\nu_d}{r_*^2 D} \sqrt{\frac{2\pi}{\varphi_m''}}\, e^{-E_m}, \tag{A13}$$

$$q = \left(\frac{r_m}{r_*}\right)^2. \tag{A14}$$

Eqs. A8–A14 are the dimensional versions of Eqs. 68–78 from Neu and Krassowska. Energies E, φ, and U are in units of kT, and U_*', φ_*', and φ_m'' denote derivatives with respect to r evaluated at r_* and r_m.

In application to a single cell, the following simplifications were made. First, the formulation given above represents a quasistatic limit, i.e., it is assumed that the pore distribution function n adjusts instantaneously to temporal variations in pore energy. As argued in the original study (Neu and Krassowska, 1999), this approximation is valid when the changes in V_m occur on a time scale of at least 5 μs. Here, cellular polarization has a time constant of 1.1 μs, so the quasistatic approximation introduces an error. However, since this assumption affects only the coefficient N_o, one can expect only a modest difference between solutions using the quasistatic and time dependent versions of the asymptotic ODE.

Second, the model used here suppresses the dependence of α and N_o on the transmembrane potential and treats them as constants. This simplification is acceptable because the dependence of dN/dt on V_m is dominated by the exponential $\exp[(V_m/V_{ep})^2]$. In comparison, the dependence on V_m through α and N_o is much weaker and is unlikely to be detectable experimentally. The radius at the minimum pore energy r_m also depends on V_m, but it changes very little for V_m between 0 mV and the critical value V_{cr} (Neu and Krassowska, 1999). Hence, r_m and, consequently, q are constant.

In principle, Eqs. A11–A14 can be used to determine values for the parameters of the model. However, this method would use several molecular-level constants whose values are known only up to an order of magnitude (Barnett and Weaver, 1991). Alternatively, the four parameters can be determined experimentally. Glaser et al. (1988) performed specially designed voltage-clamp experiments on artificial lipid bilayers that yielded estimates for α and V_{ep}. The single cell model adopted Glaser's value for α, but decreased V_{ep} from 460 to 258 mV so that $V_{cr} \approx 1$ V, the value reported by Kinosita and coworkers for unfertilized sea urchin eggs (Hibino et al., 1991, 1993; Kinosita et al., 1988, 1991, 1992). N_o was computed by dividing the measured background conductivity of a lipid bilayer by the conductance of a single pore (Benz and Hancock, 1981; Chernomordik and Chizmadzhev, 1989; Rosenberg and Jendrasiak, 1968). Finally, q was chosen based on the experimental estimates of Glaser and coworkers for r_* (0.3–0.5 nm) and r_m (0.6–1.0 nm) (Glaser et al., 1988).

APPENDIX B: SINGULAR PERTURBATION APPROXIMATION TO EQS. 1–4

For the pore resealing phase, this study uses singular perturbation to develop approximate, quasistationary equations governing the intracellular and extracellular potentials Φ_i and Φ_e. Once the shock has ceased and the induced potential has been discharged, V_m assumes a nearly constant value V_* everywhere around the cell,

$$V_* = \frac{g_l E_l}{g_l + G_*} \approx -0.178 \text{ mV}, \tag{B1}$$

where $G_* = 89.32$ mS/cm^2 is the average conductance of the electroporated membrane as determined from simulations. G_* is due to pores remaining in the membrane after the shock, as they reseal with a time constant $\tau_N = 1.5$ s (Eq. 11). Recognizing that τ_N is 10^6 times larger than the cellular time constant $\tau_c = 1.1$ μs (Eq. 9) motivates the use of singular perturbation. The method used here is similar to the one proposed for an excitable cell in an external electric field (Krassowska and Neu, 1994). The first step is to convert the governing equations into nondimensional form using the system of units shown in Table B1. Equations 1–3 remain unchanged because they are invariant under scaling. Equation 4 for the boundary conditions on the membrane S is written as

$$-\hat{n} \cdot \nabla \Phi_i = -\hat{n} \cdot (\mu \nabla \Phi_e) = \varepsilon \frac{\partial \Phi_m}{\partial t} + \kappa I_{ion} + \nu I_{ep} \quad \text{on } S, \tag{B2}$$

where $\mu \equiv \sigma_e/\sigma_i$, $\kappa \equiv g_l N_o/\alpha C_m$, and $\nu \equiv d_c G_*/\sigma_i$ are $O(1)$ constants and $\varepsilon \equiv \tau_c/\tau_N = d_c \alpha C_m/\sigma_i N_o = 1.4 \times 10^{-6}$ is a small parameter. The presence of this small parameter in Eq. B2 allows the expansion of potentials in powers of ε. For Φ_i,

$$\Phi_i(\mathbf{x}, t, \varepsilon) \sim \phi_i^0 + \varepsilon \phi_i^1 \quad \text{in the intracellular space } \Omega_i, \tag{B3}$$

and similar expansions are written for Φ_e and Φ_m. Substituting these expansions into Eqs. 1 and B2 gives

$$\nabla^2(\phi_i^0 + \varepsilon \phi_i^1) = 0 \quad \text{in } \Omega_i, \tag{B4}$$

TABLE B1 Singular perturbation scaling units

Parameter	Unit	Typical Value
x	$d_c = 2a$	100 μm
t	N_o/α	1.5 s
σ_i, σ_e	σ_i	4.55 mS/cm
V_m	V_*	−0.178 mV
I_{ion}	$g_l(V_* - V_{rest})$	15.9 μA/cm^2
I_{ep}	$G_* V_*$	−15.9 μA/cm^2

$$-\hat{n}\cdot\nabla(\phi_i^0+\varepsilon\phi_i^1) = \varepsilon\frac{\partial}{\partial t}(\phi_m^0+\varepsilon\phi_m^1)+\kappa I_{ion}+\nu I_{ep} \quad \text{on } S. \tag{B5}$$

Since $\varepsilon \sim 10^{-6}$, only the leading order terms will be considered. The contribution of the first-order terms is less than 0.1% as determined by simulations. Collecting powers of ε and discarding all but the leading order terms results in a simplified system of equations governing ϕ_i^0,

$$\nabla^2\phi_i^0 = 0 \quad \text{in } \Omega_i, \tag{B6}$$

$$-\hat{n}\cdot\nabla\phi_i^0 = \kappa I_{ion}+\nu I_{ep} \quad \text{on } S. \tag{B7}$$

Analogous equations can be derived for the extracellular potential $\Phi_e \sim \phi_e^0$,

$$\nabla^2\phi_e^0 = 0 \quad \text{in the extracellular space } \Omega_e, \tag{B8}$$

$$-\hat{n}\cdot(\mu\nabla\phi_e^0) = \kappa I_{ion}+\nu I_{ep} \quad \text{on } S, \tag{B9}$$

$$\phi_e^0(\theta, t) = 0 \tag{B10}$$

With I_{ion} and I_{ep} known from the previous time step, the system of equations for ϕ_i^0 and ϕ_e^0 can be treated as a time-independent boundary value problem. Eqs. B6–B10 are converted to spherical coordinates and discretized in r and θ using the finite difference method. The resulting linear systems of equations is solved in each time step using Gaussian elimination. The transmembrane potential is computed from ϕ_i^0 and ϕ_e^0 and used to update N and calculate I_{ion} and I_{ep}. The time step during resealing is governed by the convergence requirements for Eq. 8 describing the rate of change of N. With $\tau_N = 1.5$ s the maximum time step is 100 ms, and a 20 s simulation (complete resealing) can be completed in 7 minutes, 44 seconds on a Sun Ultra 1. If, instead, the original problem (Eqs. 1–4) is used, the computational time is estimated to be 1800 hours. The substantial savings of the singular perturbation approximation make it feasible to conduct investigations of the resealing process in an electroporated single cell.

This work was supported by the National Institutes of Health Grant HL54071, National Science Foundation Engineering Research Center Grant CDR-8622201, and by a Graduate Fellowship from The Whitaker Foundation.

REFERENCES

Abidor, I. G., V. B. Arakelyan, L. V. Chernomordik, Y. A. Chizmadzhev, V. F. Pastushenko, and M. R. Tarasevich. 1979. Electric breakdown of bilayer lipid membranes. I. Main experimental facts and their qualitative discussion. *Bioelectrochem. Bioenerg.* 6:37–52.

Aguel, F., K. A. DeBruin, W. Krassowska, and N. Trayanova. 1999. Effects of electroporation on the transmembrane potential distribution in a two-dimensional bidomain model of cardiac tissue. *J. Cardiovasc. Electrophysiol.* 10:701–714.

Barnett, A. 1990. The current-voltage relation of an aqueous pore in a lipid bilayer membrane. *Biochim. Biophys. Acta.* 1025:10–14.

Barnett, A. and J. C. Weaver. 1991. Electroporation: A unified, quantitative theory of reversible electrical breakdown and mechanical rupture in artificial planar bilayer membranes. *Bioelectrochem. Bioenerg.* 25: 163–182.

Benz, R., F. Beckers, and U. Zimmermann. 1979. Reversible electrical breakdown of lipid bilayer membranes: A charge-pulse relaxation study. *J. Membr. Biol.* 48:181–204.

Benz, R. and R. E. W. Hancock. 1981. Properties of the large ion-permeable pores formed from protein F of *Pseudomonas aeruginosa* in lipid bilayer membranes. *Biochim. Biophys. Acta.* 646:298–308.

Chambers, E. L. and J. de Armendi. 1979. Membrane potential, action potential and activation potential of eggs of the sea urchin, *Lytechinus variegatus. Exp. Cell. Res.* 122:203–218.

Chang, D. C. 1992. Structure and dynamics of electric field-induced membrane pores as revealed by rapid-freezing electron microscopy. *In* Guide to Electroporation and Electrofusion. D. C. Chang, B. M. Chassy, J. A. Saunders and A. E. Sowers, editors. Academic Press, Inc., New York. 9–27.

Chang, D. C., B. M. Chassy, J. A. Saunders, and A. E. Sowers, editors. 1992. Guide to Electroporation and Electrofusion. Academic Press, Inc., New York.

Chernomordik, L. V., S. I. Sukharev, I. G. Abidor, and Y. A. Chizmadzhev. 1983. Breakdown of lipid bilayer membranes in an electric field. *Biochim. Biophys. Acta.* 736:203–213.

Chernomordik, L. V. and Y. A. Chizmadzhev. 1989. Electrical breakdown of lipid bilayer membranes: phenomenology and mechanism. *In* Electroporation and Electrofusion in Cell Biology. E. Neumann, A. E. Sowers, and C. A. Jordan, editors. Plenum Press, New York. 83–95.

DeBruin, K. A. and W. Krassowska. 1998. Electroporation and shock-induced transmembrane potential in a cardiac fiber during defibrillation strength shocks. *Ann. Biomed. Eng.* 26:584–596.

DeBruin, K. A. and W. Krassowska. 1999. Modeling electroporation in a single cell. II. Effects of ionic concentrations. *Biophys. J.* 77:000–000.

Djuzenova, C. S., U. Zimmermann, H. Frank, V. L. Sukhorukov, E. Richter, and G. Fuhr. 1996. Effect of medium conductivity and composition on the uptake of propidium iodide into electropermeabilized myeloma cells. *Biochim. Biophys. Acta.* 1284:143–152.

Freeman, S. A., M. A. Wang, and J. C. Weaver. 1994. Theory of electroporation of planar bilayer membranes: Predictions of the aqueous area, change in capacitance, and pore-pore separation. *Biophys. J.* 67:42–56.

Gabriel, B. and J. Teissie. 1997. Direct observation in the millisecond time range of fluorescent molecule asymmetrical interaction with the electropermeabilized cell membrane. *Biophys. J.* 73:2630–2637.

Genco, I., A. Gliozzi, A. Relini, M. Robello, and E. Scalas. 1993. Electroporation in symmetric and asymmetric membranes. *Biochim. Biophys. Acta.* 1149:10–18.

Glaser, R. W., S. L. Leikin, L. V. Chernomordik, V. F. Pastushenko, and A. I. Sokirko. 1988. Reversible electrical breakdown of lipid bilayers: formation and evolution of pores. *Biochim. Biophys. Acta.* 940:275–287.

Gross, D., L. M. Loew, and W. W. Webb. 1986. Optical imaging of cell membrane potential changes induced by applied electric fields. *Biophys. J.* 50:339–348.

Hibino, M., M. Shigemori, H. Itoh, K. Nagayama, and K. Kinosita. 1991. Membrane conductance of an electroporated cell analyzed by submicrosecond imaging of transmembrane potential. *Biophys. J.* 59:209–220.

Hibino, M., H. Itoh, and K. Kinosita. 1993. Time courses of cell electroporation as revealed by submicrosecond imaging of transmembrane potential. *Biophys. J.* 64:1789–1800.

Isambert, H. 1998. Understanding the electroporation of cells and artificial lipid bilayers. *Phys. Rev. Lett.* 80:3404–3407.

Israelachvili, J. 1992. Intermolecular and Surface Forces, Academic Press, London, UK.

Jones, J. L., E. Lepeschkin, R. E. Jones, and S. Rush. 1978. Response of cultured myocardial cells to countershock-type electric field stimulation. *Am. J. Physiol.* 235:H214–H222.

Jones, J. L., R. E. Jones, and G. Balasky. 1987. Microlesion formation in myocardial cells by high-intensity electric field stimulation. *Am. J. Physiol.* 253:H480–H486.

Kinosita, K. and T. Y. Tsong. 1979. Voltage-induced conductance in human erythrocyte membranes. *Biochim. Biophys. Acta.* 554:479–497.

Kinosita, K., I. Ashikawa, N. Saita, H. Yoshimura, H. Itoh, K. Nagayama, and A. Ikegami. 1988. Electroporation of cell membrane visualized under a pulsed-laser fluorescence microscope. *Biophys. J.* 53: 1015–1019.

Kinosita, K., H. Itoh, S. Ishiwata, K. Hirano, T. Nishizaka, and T. Hayakawa. 1991. Dual-view microscopy with a single camera: real-time imaging of molecular orientations and calcium. *J. Cell Biol.* 115:67–73.

Kinosita, K., M. Hibino, H. Itoh, M. Shigemori, K. Hirano, Y. Kirino, and T. Hayakawa. 1992. Events of membrane electroporation visualized on a time scale from microseconds to seconds. *In* Guide to Electroporation

and Electrofusion. D. C. Chang, B. M. Chassy, J. A. Saunders, and A. E. Sowers, editors. Academic Press, Inc., New York. 29–46.

Knisley, S. B. 1994. Transmembrane potentials at the ends of ventricular myocytes during electroporation by field stimulation. *PACE.* 17:838.

Knisley, S. B. and A. O. Grant. 1995. Asymmetrical electrically induced injury of rabbit ventricular myocytes. *J. Mol. Cell. Cardiol.* 27: 1111–1122.

Krassowska, W. and J. C. Neu. 1994. Response of a single cell to an external electric field. *Biophys. J.* 66:1768–1776.

Krassowska, W. 1995. Effects of electroporation on transmembrane potential induced by defibrillation shocks. *PACE.* 18:1644–1660.

Lojewska, Z., D. L. Farkas, B. Ehrenberg, and L. M. Loew. 1989. Analysis of the effect of medium and membrane conductance on the amplitude and kinetics of membrane potentials induced by externally applied electric fields. *Biophys. J.* 56:121–128.

Mehrle, W., U. Zimmermann, and R. Hampp. 1985. Evidence for asymmetrical uptake of fluorescent dyes through electro-permeabilized membranes of *Avena* mesophyll protoplasts. *Fed. Eur. Biochem. Soc.* 185: 89–94.

Mehrle, W., R. Hampp, and U. Zimmermann. 1989. Electric pulse induced membrane permeabilisation. Spatial orientation and kinetics of solute efflux in freely suspended and dielectrophoretically aligned plant mesophyll protoplasts. *Biochim. Biophys. Acta.* 978:267–275.

Neu, J. C. and W. Krassowska. 1999. Asymptotic model of electroporation. *Phys. Rev. E.* 59:3471–3482.

Neumann, E., A. E. Sowers, and C. A. Jordan, editors. 1989. Electroporation and Electrofusion in Cell Biology. Plenum Press, New York.

Neumann, E., A. Sprafke, E. Boldt, and H. Wold. 1992. Biophysical considerations of membrane electroporation. *In* Guide to Electroporation and Electrofusion. D. C. Chang, B. M. Chassy, J. A. Saunders, and A. E. Sowers, editors. Academic Press, Inc., New York. 77–90.

Pastushenko, V. F., Y. A. Chizmadzhev, and V. B. Arakelyan. 1979. Electric breakdown of bilayer lipid membranes. II. Calculation of the membrane lifetime in the steady-state diffusion approximations. *Bioelectrochem. Bioenerg.* 6:53–62.

Powell, K. T. and J. C. Weaver. 1986. Transient aqueous pores in bilayer membranes: a statistical theory. *Bioelectrochem. Bioenerg.* 15:211–227.

River, L. P., R. C. Lee, and F.-S. Pan. 1991. Evidence for electroporation mediated cellular injury in vivo. *Proc. 13th Annual Conf. of the IEEE Engineering in Medicine and Biology Society.* Institute of Electrical and Electronics Engineers, Inc., Piscataway, NJ. 1008–1009.

Rosenberg, B. and G. L. Jendrasiak. 1968. Semiconductive properties of lipids and their possible relationship to lipid bilayer conductivity. *Chem. Phys. Lipids.* 47–54.

Rossignol, D. P., G. L. Decker, W. J. Lennarz, T. Y. Tsong, and J. Teissie. 1983. Induction of calcium-dependent, localized cortical granule breakdown in sea-urchin eggs by voltage pulsation. *Biochim. Biophys. Acta.* 763:346–355.

Schwann, H. P. 1989. Dielectrophoresis and rotation of cells. *In* Electroporation and Electrofusion in Cell Biology. E. Neumann, A. E. Sowers, and C. A. Jordan, editors. Plenum Press, New York. 3–21.

Tekle, E., R. D. Astumian, and P. B. Chock. 1990. Electro-permeabilization of cell membranes: effect of the resting membrane potential. *Biochem. Biophys. Res. Comm.* 172:282–287.

Tekle, E., R. D. Astumian, and P. B. Chock. 1994. Selective and asymmetric molecular transport across electroporated cell membranes. *Proc. Natl. Acad. Sci. USA.* 91:11512–11516.

Teruel, M. N. and T. Meyer. 1997. Electroporation-induced formation of individual calcium entry sites in the cell body and processes of adherent cells. *Biophys. J.* 73:1785–1796.

Tovar, O. and L. Tung. 1992. Electroporation and recovery of cardiac cell membrane with rectangular voltage pulses. *Am. J. Physiol.* 263: H1128–H1136.

Tsong, T. Y. 1991. Electroporation of cell membranes. *Biophys. J.* 60: 297–306.

Tung, L., O. Tovar, M. Neunlist, S. K. Jain, and R. J. O'Neill. 1995. Effects of strong electrical shocks on cardiac muscle tissue. *Ann. N.Y. Acad. Sci.* 720:160–175.

Weaver, J. C. and R. A. Mintzer. 1981. Decreased bilayer stability due to transmembrane potentials. *Phys. Lett.* 86A:57–59.

Weaver, J. C. and A. Barnett. 1992. Progress toward a theoretical model for electroporation mechanism: membrane electrical behavior and molecular transport. *In* Guide to Electroporation and Electrofusion. D. C. Chang, B. M. Chassy, J. A. Saunders, and A. E. Sowers, editors. Academic Press, Inc., New York. 95–117.

Weaver, J. C. and Y. A. Chizmadzhev. 1996. Theory of electroporation: a review. *Bioelectrochem. Bioenerg.* 41:135–160.

Zhang, L., L. Li, G. A. Hofmann, and R. M. Hoffmann. 1996. Depth-targeted efficient gene delivery and expression in the skin by pulsed electric fields: an approach to gene therapy of skin aging and other diseases. *Biochem. Biophys. Res. Comm.* 220:633–636.

Zhou, X., W. M. Smith, D. L. Rollins, and R. E. Ideker. 1996. Transmembrane potential changes caused by shocks in guinea pig papillary muscle. *Am. J. Physiol.* 271:H2536–H2546.

Zimmermann, U. 1982. Electric field-mediated fusion and related electrical phenomena. *Biochim. Biophys. Acta.* 694:227–277.